

共同利用実施報告書(研究実績報告書)  
(一般共同研究)

1. 課題番号 2014-G-02

2. 研究課題名 (和文、英文の両方をご記入ください)

和文：海洋／固体地球システム現象解明のための高感度絶対水圧計海底アレー観測

英文：Ocean bottom array observation with high resolution absolute pressure gauges to explore coupled phenomena of the ocean and solid Earth \_\_\_\_\_

3. 研究代表者所属・氏名 海洋研究開発機構・深尾良夫

(地震研究所担当教員名) 塩原 肇

4. 参加者の詳細 (研究代表者を含む。必要に応じ行を追加すること)

氏名	所属・職名	参加内容
深尾良夫	海洋研究開発機構・特任上席研究員	研究統括
杉岡裕子	海洋研究開発機構・主任研究員	観測
利根川貴志	海洋研究開発機構・研究員	解析
塩原 肇	東京大学地震研究所・教授	装置改良整備
篠原雅尚	東京大学地震研究所・教授	装置改良整備
西田 究	東京大学地震研究所・准教授	解析

5. 研究計画の概要 (申請書に記載した「研究計画」を800字以内でご記入ください。変更がある場合、変更内容が分かるように記載してください。)

#### 1) 研究目的と意義

周期数秒から数日程度にわたる広い帯域で海洋変動と海底下固体地球変動を海底から同時に見る目的での高分解能絶対水圧計アレー観測システムを製作し、以下の観測研究を実施する。**1.** 小笠原海嶺の東側裾野にアレーを展開し内部潮汐波をモード分離して抽出する。**2.** 低角逆断層地震活動の稀な小笠原海域において、こうした地震がよく起こる特異な場所にアレーを展開し、海洋レーリー波エアリー相に着目して地震より長い時定数のプレート境界滑りを検出する。**3.** 常時地球自由振動の励起源である長周期海洋重力波記録の相関解析を行いその発生源を特定する。特に H26 年度共同研究においては、高分解能絶対水圧観測システムの改良と最初の実機 10 台の小笠原海域への投入を行う。併せて広帯域海底地震計 1 台を投入し、将来の海底地動と海底絶対水圧との同時観測に向けてノーハウを蓄積する。

#### 2) 地震研究所の研究活動との関連性

これまで地震研究所では自ら開発してきた広帯域海底地震計を用いて主として地震学的目的に沿った観測が行われてきた。今回の共同研究は、内容的には地震学的目的に海洋物理学的目的を加え、手法的には海底地動観測に海底水圧変動観測を加えて、海底観測の内容をより豊かにしようとするものである。

#### 3) 地震研究所の施設・装置・データ等の利用

使用する観測システムは、塩原（地震研究所）の独自開発によるロガーをチタン製耐圧容器（直径 50cm、音響トランスポンダ込み）に納め、水中ケーブルを介して高分解能絶対水圧計に接続するもので、チタン製耐圧容器の部分について地震研究所所有の器材の貸与（10 台分）を希望する。

#### 4) 経費の使用目的

本研究の主要経費は科研費基盤研究 A 「海底圧力計アレー観測による海洋／固体地球システム現象の解明」（研究代表者：深尾良夫、平成 25 年度開始）：4 年間（合計 3490 万円）から支出される。借り受ける耐圧容器は一部にオーバーホールが必要でありそのために本共同研究経費を計上する。

## 6. 研究成果の概要 (図を含めて1頁で記入してください。)

キーワード(3~5程度): 海底圧力観測・海洋内部潮汐・海洋長周期重力波・プレート境界滑り

### 1. 海底観測の開始:

海洋研究開発機構所有の船舶利用に公募枠で申請し採択された。船舶名は「よこすか」、航海番号は「YK-1047」、航海期間は2014年5月12日から5月15日までの4日間。実施内容は以下の通り。

- (1) 高分解能水圧計の設置: 観測対象域の海底に10台の高感度水圧計を、最小単位が1辺10kmの正三角形、最大単位が1辺30kmの正三角形のアレーを形成するように展開した。アレーの中心観測点には広帯域海底地震計と高感度差圧計とをセットにしたシステムも設置した。また広帯域海底地震計設置点(1点)と海底圧力計設置点(10点)について、記録開始を確認した。またそれぞれの点で3点音響測距により精確な位置決めを行った。
- (2) XCTD計測: 水圧計を設置した10観測点で海中の正確な構造を知るため、XCTD計測を実施した。
- (3) 海底地形調査観測: マルチビーム音響測深機による海底地形調査を時間の許す範囲で実施した。
- (4) ADCP観測: 調査中ADCP観測を実施した。

### 2. 海底観測装置の整備:

- (1) OBPに使用した50cmチタン球の整備: 1999年以前から使用開始していたこれらのチタン球のオーバーホールを実施し、本研究で10台展開したOBPシステムの耐圧容器として使用した。これにより確実な運用が可能となったものと期待される。設置は2014年5月、今年5月に回収と船上での再整備(設置準備)を行い、引き続き1年間の観測に適用する。
- (2) 今年度の精密水圧と高精度流速の同時観測に向けた準備: JAMSTEC保有の高精度電磁流速計を上記観測に適用させるため、流速計システムの耐圧容器に水中コネクタを追加加工して取り付け、チタン球耐圧容器から外部給電可能とした。これによりやっと、1年間の平行観測を可能とした。これも今年5月の2期目の観測で設置する。

### 3. DONET水圧計ネットワークデータを用いた予備的解析:

海洋研究開発機構の海底ネットワークDONETの水圧計アレーは、センサー自身は今回の観測で使用した水圧計と同じParoScientific社の製品なので、今回の観測で得られる筈のデータで何が得られるかをテストするのに絶好である。DONET水圧計ネットワークデータを使って以下の2種の解析を実施している。

#### (1) 長周期海洋重力波の発生源の探索

研究計画・目的に記載した「**3**. 常時地球自由振動の励起源である長周期海洋重力波記録の相関解析を行いその発生源を特定する」研究を実施し、その第1報をEPSに発表した。

#### (2) 海洋内部潮汐波の検出

研究計画・目的に記載した「**1**. 小笠原海嶺の東側裾野にアレーを展開し内部潮汐波をモード分離して抽出する」研究を開始した。まだ解析初期段階であるが、3年間分の記録を通じてM2潮汐帯域で常に水平伝播速度1.9 m/sの信号が検出され、これがM2内部潮汐波の最低次モードである可能性は高い。今後、海洋物理の専門家との連携を進める予定である。

7. 研究実績（論文タイトル、雑誌・学会・セミナー等の名称、謝辞への記載の有無）下線は共同研究メンバー

(1) Fukao, Y., Seafloor array observation of water pressure, Cruise Report YK14-07, JAMSTEC, 2014. (謝辞無)

(2) Tono, Y., K. Nishida, Y. Fukao, A. To, N. Takahashi, Source characteristics of ocean infragravity waves in the Philippine Sea: Analysis of three-year continuous network records of seafloor motion and pressure, Earth, Planets and Space, 66:99, Doi:10.1186/1180-5981-66-99, 2014. (謝辞無)



Yokosuka+ “Cruise Report”

YK14-07

Ocean bottom pressure gauge array observation

Off east of Aogashima

May12, 2014-May15,2014

Japan Agency for Marine-Earth Science and Technology

(JAMSTEC)

## Contents

1. Cruise Information

2. Researchers

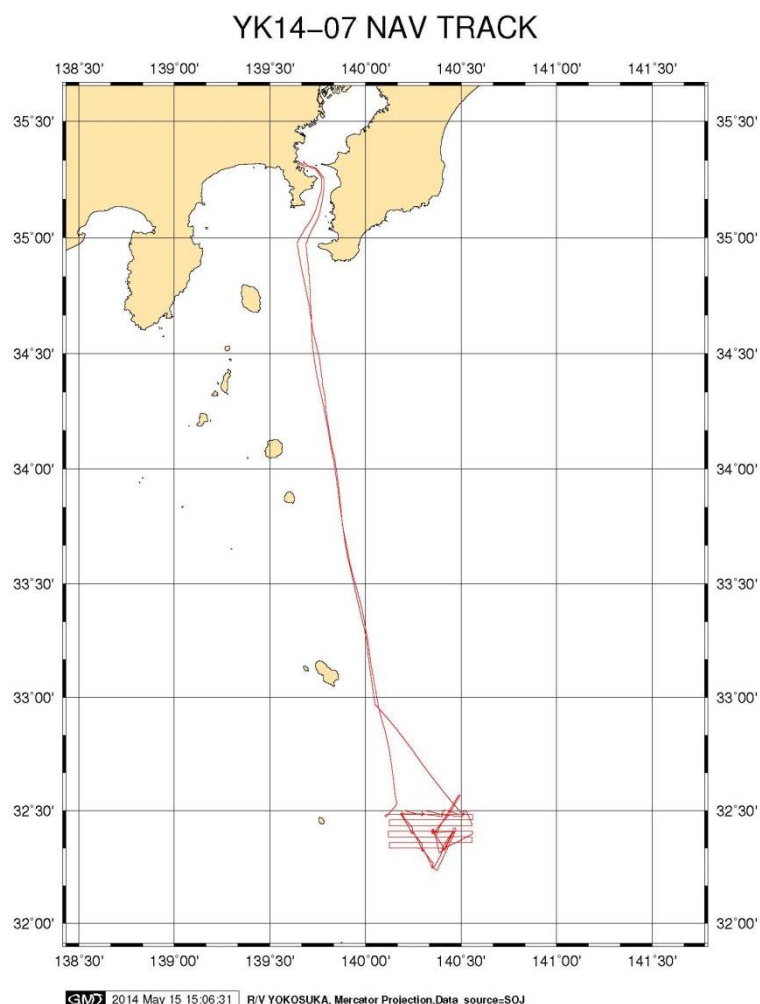
3. Observation

4. Notice on Using

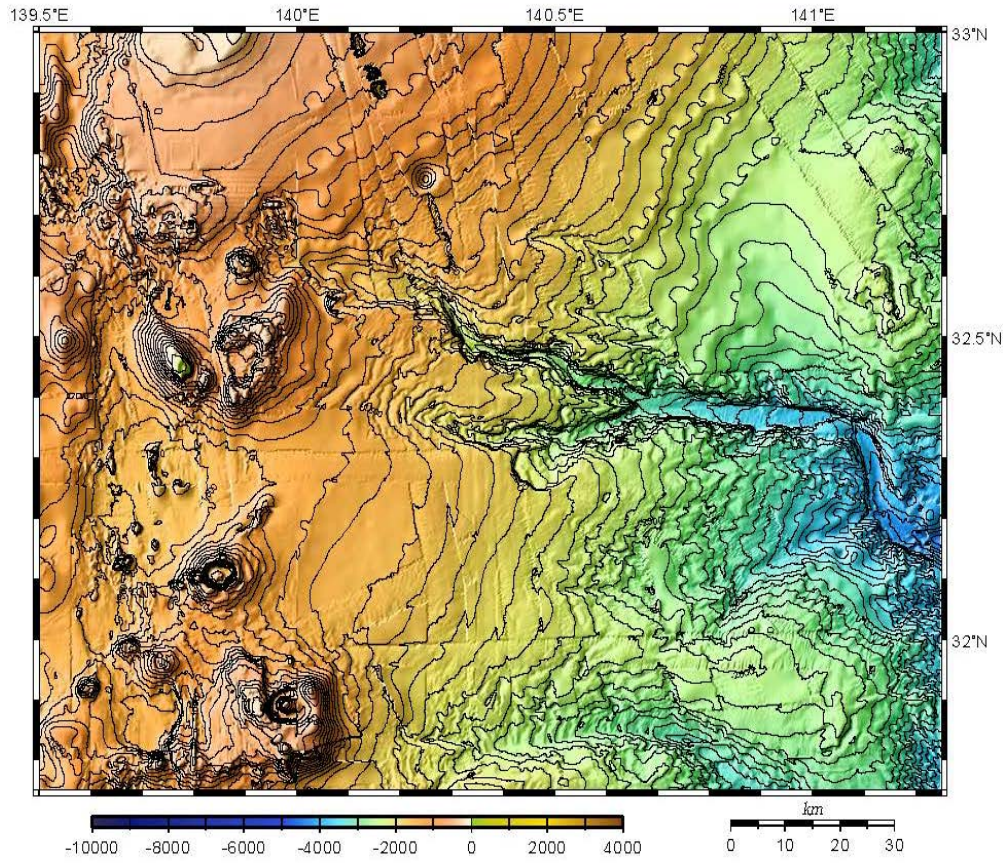
## 1. Cruise Information

- Cruise ID: YK14-07
- Name of vessel: Yokosuka
- Title of the cruise: Ocean bottom pressure gauge array observation
- Title of proposal: Study of ocean-solid Earth system by ocean bottom pressure gauge array observation
- Cruise period: May 12, 2014 – May 15, 2014
- Ports of call: JAMSTEC Pier – Sumiju Port
- Research area: Off east of Aogashima
- Research Map

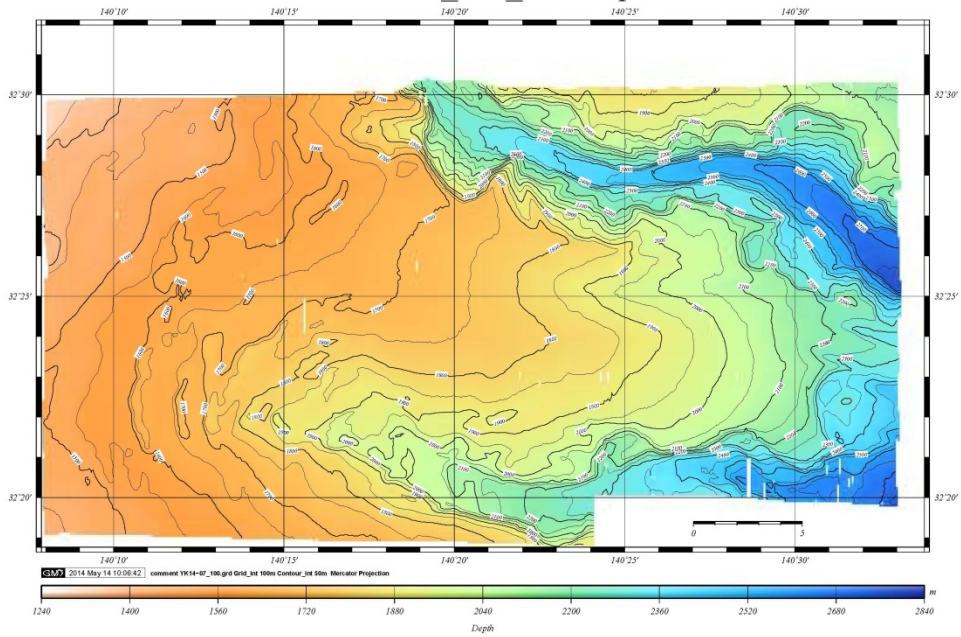
Cruise track:



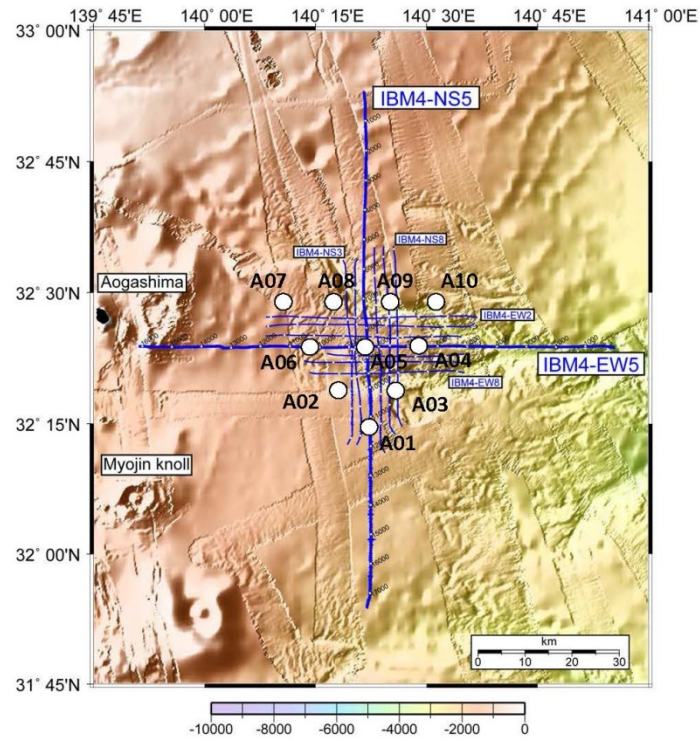
# Survey Area



YK14-07\_100\_cl50A3.ps



Observation points



設置点	時刻 (JST)	母船緯度	母船経度	水深 (m)	流向・流速
2014/5/13					
A10 OBP 投入	6:16:23	32-28.9644N	140-30.5870E	2228m	
A10 XCTD 投入	6:23:22	32-28.9307N	140-30.1760E	2258m	
A9 OBP 投入	7:07:21	32-28.9457N	140-24.1976E	1997m	
A9 XCTD 投入	7:12:05	32-28.9241N	140-23.9784E	2007m	投入/潮流→ 82.3, 0.6
A8 OBP 投入	7:56:09	32-28.9585N	140-17.8223E	1779m	投入/潮流→133.4, 0.7
A8 XCTD 投入	8:00:03	32-28.9206N	140-17.6902E	1767m	投入/潮流→155.8, 0.6
A7 OBP 投入	8:46:02	32-28.9449N	140-11.3897E	1468m	投入/潮流→175.6, 0.8
A7 XCTD 投入	8:49:04	32-28.7952N	140-11.4918E	1470m	投入/潮流→166.1, 0.7
A4 OBP 投入	9:33:02	32-24.2670N	140-14.5881E	1675m	投入/潮流→ 70.3, 1.0
A4 XCTD 投入	9:36:07	32-24.1777N	140-14.6868E	1687m	投入/潮流→ 78.8, 1.0
A2 OBP 投入	10:26:12	32-19.5637N	140-17.7971E	1771m	投入/潮流→104.1, 0.9
A2 XCTD 投入	10:29:19	32-19.4552N	140-17.9397E	1758m	投入/潮流→104.1, 1.1
A1 OBP 投入	11:17:08	32-14.9605N	140-21.0044E	1745m	投入/潮流→ 79.7, 0.9
A1 XCTD 投入	11:19:19	32-14.8726N	140-21.0995E	1747m	投入/潮流→ 87.2, 0.9
A6 OBP 投入	12:45:47	32-24.2717N	140-27.3954E	1973m	投入/潮流→113.0, 0.9
A6 XCTD 投入	12:48:17	32-24.1840N	140-27.3346E	1968m	投入/潮流→133.8, 0.8
A3 OBP 投入	13:37:22	32-19.5686N	140-24.2051E	2184m	投入/潮流→124.6, 0.6
A3 XCTD 投入	13:40:03	32-19.4856N	140-24.1583E	2155m	投入/潮流→157.5, 0.5
A5 OBP 投入	14:47:21	32-24.2612N	140-20.9697E	1759m	投入/潮流→156.9, 0.5
A5 BBOBS 投入	14:54:15	32-24.2787N	140-20.9741E	1754m	投入/潮流→150.1, 0.5
A5 XCTD 投入	14:58:04	32-24.2379N	140-21.0105E	1756m	投入/潮流→150.6, 0.6

## 2. Researchers

- Chief scientist: Yoshio Fukao (JAMSTEC)
- Representative of the science party: Yoshio Fukao (JAMSTEC)
- Science party (List) :

Yoshio Fukao (JAMSTEC), Planning, Observational support  
Hiroko Sugioka (JAMSTEC), Preparation, Installation  
Aki Ito (JAMSTEC), Preparation, Installation

### 3. Observation

- Overview of the observation

We have so far developed an array system of high resolution ocean bottom pressure gauges to observe phenomena occurring above and below the seafloor simultaneously. We deployed this system on the seafloor off coast of Aogashima Island to observe, among others, internal tides, ocean infragravity waves and low-frequency earthquakes for about a year period from May 13, 2013. This observation is expected to retrieve signals of low order internal tides and to obtain information about the sources of infragravity waves.

- Activities

- (1) Deployment of 10 high resolution pressure gauges and a BBOBS

We placed 10 high resolution pressure gauges in an equilateral triangle with a side 30 km that consists of 9 smallest equilateral triangles with a side 10 km long. At the central site of this array we also deployed a set of broadband ocean bottom seismometer and a high resolution differential pressure gauges. At each of 10 pressure gauge stations and a broadband seismic station we confirmed that the instrument started recording. We also conducted echo ranging to determine its precise position.

- (2) XCTD measurements

At each of the ten observational sites we conducted XCTD measurement to extract information about the 1D structure of the ocean.

- (3) Seafloor topographic survey

A seafloor topographic survey was done by multi-beam echo sounding. The amount of data was limited, however, because we had to shorten the schedule to escape from an approaching storm.

- (4) ADCP survey

During the navigation an ADCP survey was done to extract information about ocean current.

## Detail

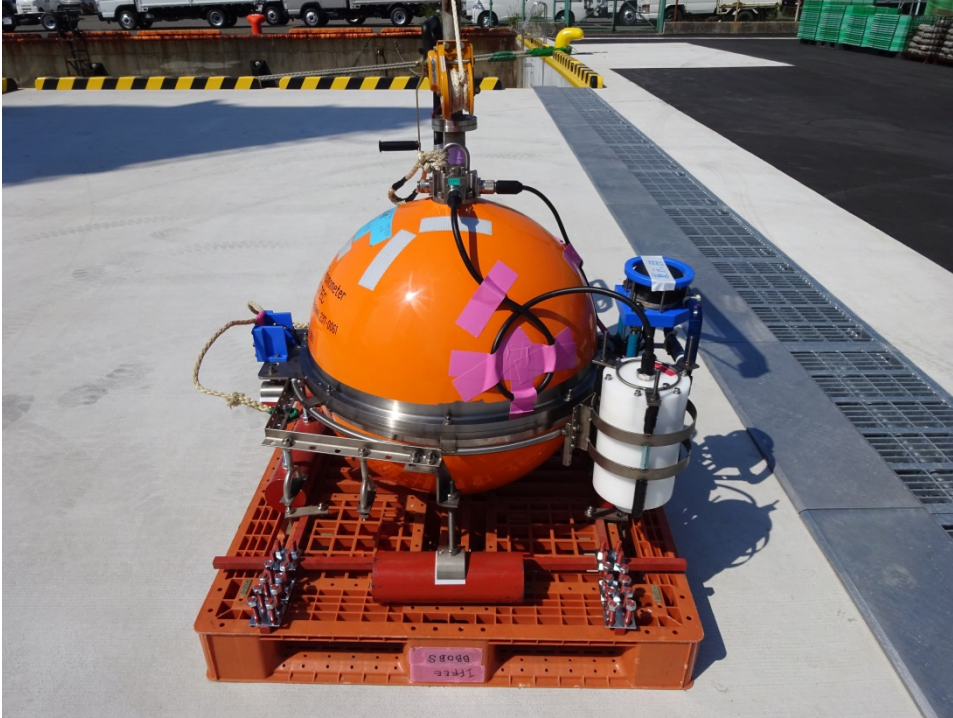
日付 Date	時間 Local Time	内容 Note	特記事項 Description	本船位置／気象／海象 Position/Weather/Wind/Sea condition
12-May-14		<b>Sail out, proceeding to research area</b>		5/12 12:00 (UTC+9h)
	08:00	boarded		34-43.4'N, 139-42.2'E
	09:00	Proceeding to research area		East off Oshima
	10:00-10:30	Briefing about ship's life and safety		c (Cloudy)
	16:30-17:00	Meeting (R/V YOKOSUKA Crew and Scientist).		SW-5 (Fresh breeze)
	23:00	Arrived at research area.		3 (Sea slight)
	23:01	Released XBT at <32-32.7062'N, 140-09.6134'E>		1 (Low swell short or average)
	23:48	Commenced MBES survey.		Visibly: 7'
13-May-14		<b>Deploy OBP &amp; BBOBS at site A01-A10</b>		5/13 12:00 (UTC+9h)
	05:48	Finished MBES survey.		32-19.5'N, 140-25.4'E
	06:16	Deployed OBP at site A10 (32-28.9644'N, 140-30.5870'E)	depth: 2228.4m	East off Aogashima
	06:23	Released XCTD at site A10 (32-28.9307'N, 140-30.1760'E)	depth: 2258.2m	r (Rain)
	07:07	Deployed OBP at site A09 (32-28.9457'N, 140-24.1976'E)	depth: 1997.1m	S-7(Near gale)
	07:12	Released XCTD at site A09 (32-28.9241'N, 140-23.9784'E)	depth: 2007.4m	5 (Sea rough)
	07:56	Deployed OBP at site A08 (32-28.9585'N, 140-17.8223'E)	depth: 1779.2m	4 (Moderate average)
	08:00	Released XCTD at site A08 (32-28.9206'N, 140-17.6902'E)	depth: 1767.0m	Visibly: 2'
	08:46	Deployed OBP at site A07 (32-28.9449'N, 140-11.3897'E)	depth: 1467.7m	

	08:49	Released XCTD at site A07 (32-28.7952'N, 140-11.4918'E)	depth: 1469.9m	
	09:33	Deployed OBP at site A04 (32-24.2670'N, 140-14.5881'E)	depth: 1675.4m	
	09:36	Released XCTD at site A04 (32-24.1777'N, 140-14.6868'E)	depth: 1686.8m	
	10:26	Deployed OBP at site A02 (32-19.5637'N, 140-17.7971'E)	depth: 1771.0m	
	10:29	Released XCTD at site A02 (32-19.4552'N, 140-17.9397'E)	depth: 1757.9m	
	11:17	Deployed OBP at site A01 (32-14.9605'N, 140-21.0044'E)	depth: 1744.8m	
	11:19	Released XCTD at site A01 (32-14.8726'N, 140-21.0995'E)	depth: 1747.3m	
	12:45	Deployed OBP at site A06 (32-24.2717'N, 140-27.3954'E)	depth: 1973.0m	
	12:48	Released XCTD at site A06 (32-24.1840'N, 140-27.3346'E)	depth: 1968.2m	
	13:37	Deployed OBP at site A03 (32-19.5686'N, 140-24.2051'E)	depth: 2184.1m	
	13:40	Released XCTD at site A03 (32-19.4856'N, 140-24.1583'E)	depth: 2154.6m	
	14:47	Deployed OBP at site A05 (32-24.2612'N, 140-20.9697'E)	depth: 1759.1m	
	14:54	Deployed BBOBS at site A05 (32-24.2787'N, 140-20.9741'E)	depth: 1753.9m	
	14:58	Released XCTD at site A05 (32-24.2379'N, 140-21.0105'E)	depth: 1756.1m	
	21:02-22:22	Carried out confirmation of acoustic signal from OBP & BBOBS (A05).		
	22:33-23:09	Carried out confirmation of acoustic signal from OBP (A06).		
	23:53	Carried out confirmation of acoustic signal from OBP (A03).		
14-May-14		<b>Calibrate OBP &amp; BBOBS &amp; Proceeded to SUMITOMOZYUKIKAI-Quay</b>		5/14 12:00 (UTC+9h)
	00:10	Finished confirmation of acoustic signal from OBP (A03).		32-19.3'N, 140-23.9'E
	01:08	Commenced MBES survey.		East off Aogashima
	08:18	Finished MBES survey.		bc (Fine but cloudy)
	08:55-09:10	Carried out confirmation of acoustic signal from OBP & BBOBS (A05).		W-4 (Moderate breeze)

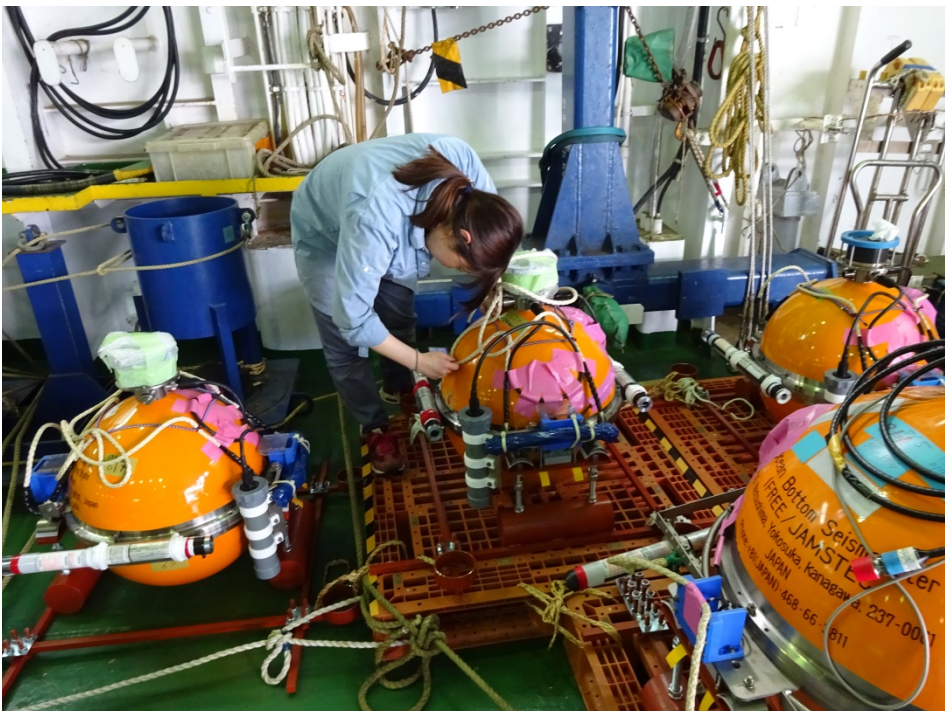
	09:15-10:02	Carried out calibration of OBP & BBOBS (A05).		3 (Sea slight)
	10:36-10:56	Carried out calibration of OBP (A06).		2 (Low swell long)
	11:32-12:10	Carried out calibration of OBP (A03).		Visibly: 7'
	12:46-13:23	Carried out calibration of OBP (A01).		
	13:57-14:34	Carried out calibration of OBP (A02).		
	15:09-15:47	Carried out calibration of OBP (A04).		
	16:20-16:53	Carried out calibration of OBP (A07).		
	17:29-18:04	Carried out calibration of OBP (A08).		
	18:46-19:21	Carried out calibration of OBP (A09).		
	20:00-20:30	Carried out calibration of OBP (A010).		
	20:45	Proceeding to YOKOSUKA-Ko.		
15-May-14		<b>Arrived at off SUMITOMOZYUKIKAI-Quay</b>		5/15 12:00 (UTC+10h)
	15:00	Disembarked at SUMITOMOZYUKIKAI-Quay.		35-19.7'N, 139-40.5'E
				YOKOSUKA-Ko No.4
		Finished YK14-07 cruise.		o (Overcast)
				NNE-4 (Moderate breeze)
				3 (Sea slight)
				1 (Low swell short or average)
				Visibly: 3'

- Instruments

BBOBS (Broadband ocean bottom seismograph) and DPG (Differential pressure gauge)



OBPs (Ocean bottom pressure gauges)



## Installation of an OBP on the seafloor



### **BBOBS employed**

Guralp CMG-3T: 100 Hz-sampling

<http://www.guralp.com/documents/DAS-030-0001.pdf#search='CMG3T'>

<https://www.passcal.nmt.edu/content/instrumentation/sensors/broadband-sensors/cm-g-3t-bb-sensor>

### **DPG employed**

DPG\_JAMSTEC: 100 Hz-sampling

[http://www.godac.jamstec.go.jp/catalog/data/doc\\_catalog/media/JAM\\_RandDsp\\_17.pdf](http://www.godac.jamstec.go.jp/catalog/data/doc_catalog/media/JAM_RandDsp_17.pdf)

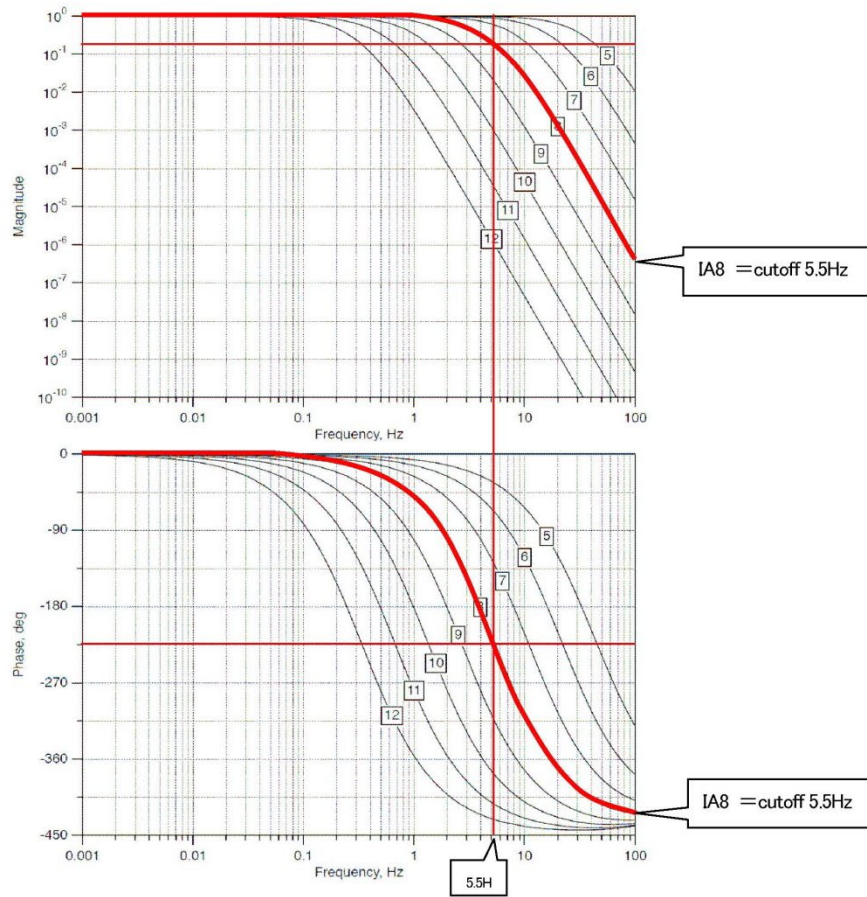
### **OBP employed**

Paroscientific 8B7000-I-005: 4 Hz-sampling

Cutoff frequency: 1.4 Hz (IA=10)

<http://www.paroscientific.com/depthsensors.htm>

<http://www.mercan.co.jp/series8000-jp.pdf#search='paroscientific'>



```

sampling frequency : fs = 1 / 28.7e-6 / 4
integer ia
real pi, f, omega, fs, delta, alpha, mag, phase, xfr, xfi
complex z, xf, xf1
alpha = 1 / (2 ^ ia)
omega = 2 * pi * f
fs = 1 / 28.7e-6 / 4
delta = 1 / fs
z = complex(cos(omega*delta), sin(omega*delta))
xf1 = 1 / (1/alpha - (1-alpha)/alpha/z)
xf = xf1 * xf1 * xf1 * xf1 * xf1
xfr = real(xf)
xfi = imag(xf)
mag = sqrt(xfr * xfr + xfi * xfi)
phase = atan(xfi / xfr)

```

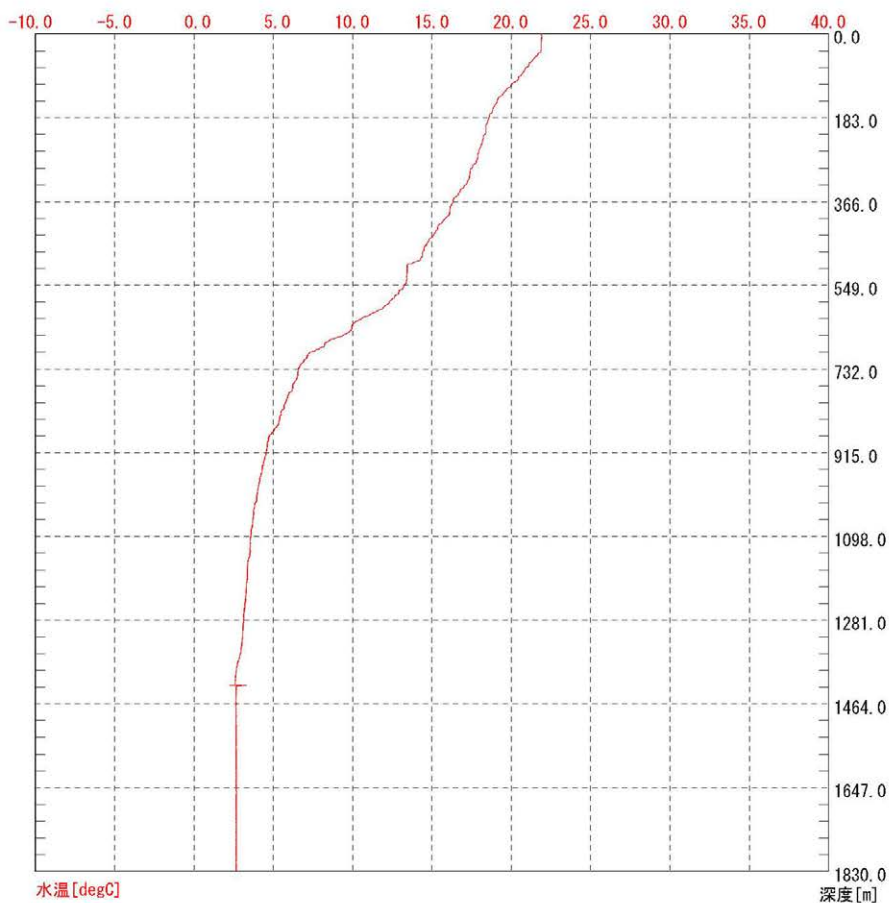
● Research results

The ocean bottom array observations have just started. We have to await a year period to recover the array system and to retrieve the records from it. Following is an example of the result of the XCTD cast that was simultaneously with the OBP installation at each observational site.

TSK XBT/XCTD-SYSTEM TS-MK130 Tsurumi-Seiki CO.,Ltd (Ver. 1.00)

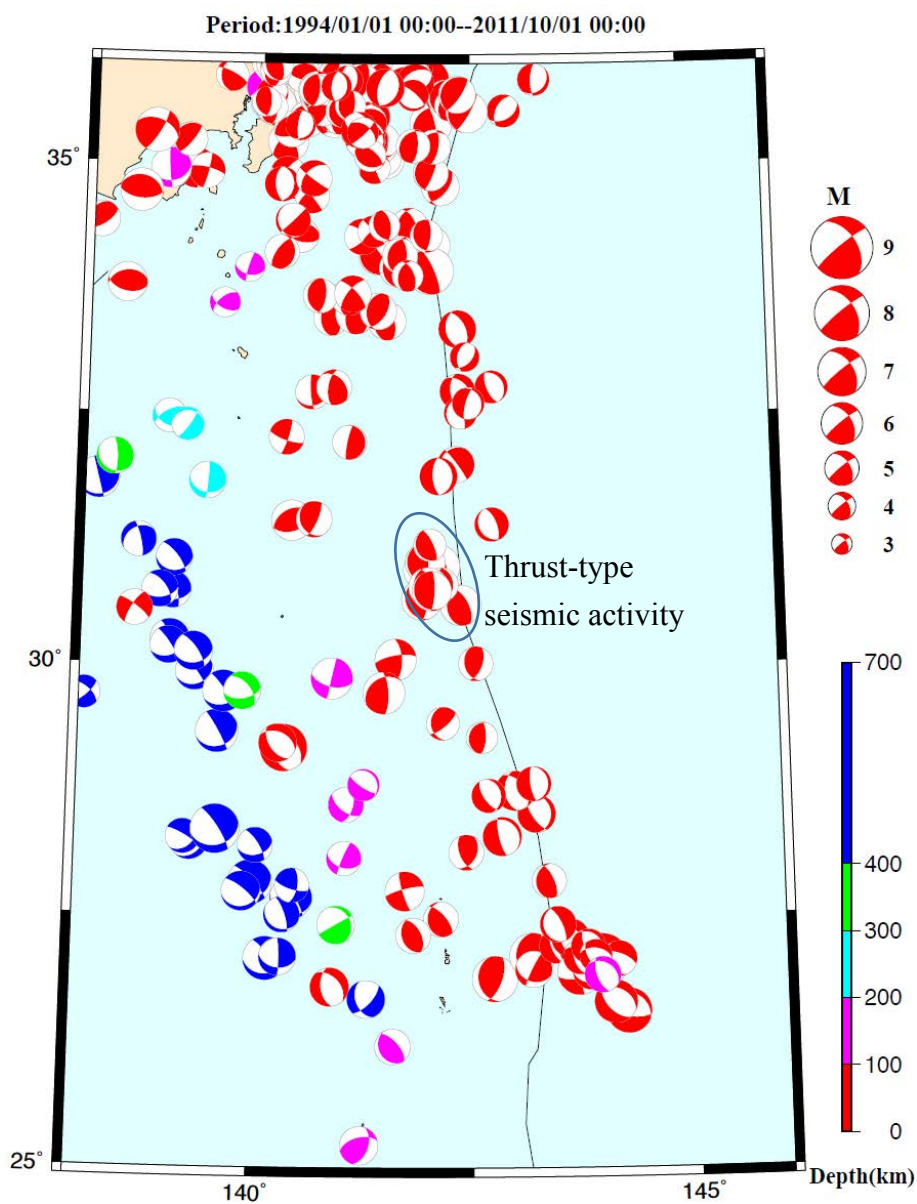
データベース名 : c:\MK-130\data¥	デバイス名 : XBT	BATHYプローブ : 231
データ名 : BT-005520140512	プローブタイプ : T05	BATHY処理器 : 43
データナンバ : 0055	深度係数 a : 6.828	
日付 : 2014/05/12	深度係数 b : -1.82	
時刻 : 14:01:15	最大深度 (m) : 1830	
緯度 : 32-32.7062N	データ数 : 1831	深度ステップ : 1m
経度 : 140-09.6134E		

TSK XBT/XCTD-SYSTEM TS-MK130 -鉛直分布図印刷- (Ver. 1.00)

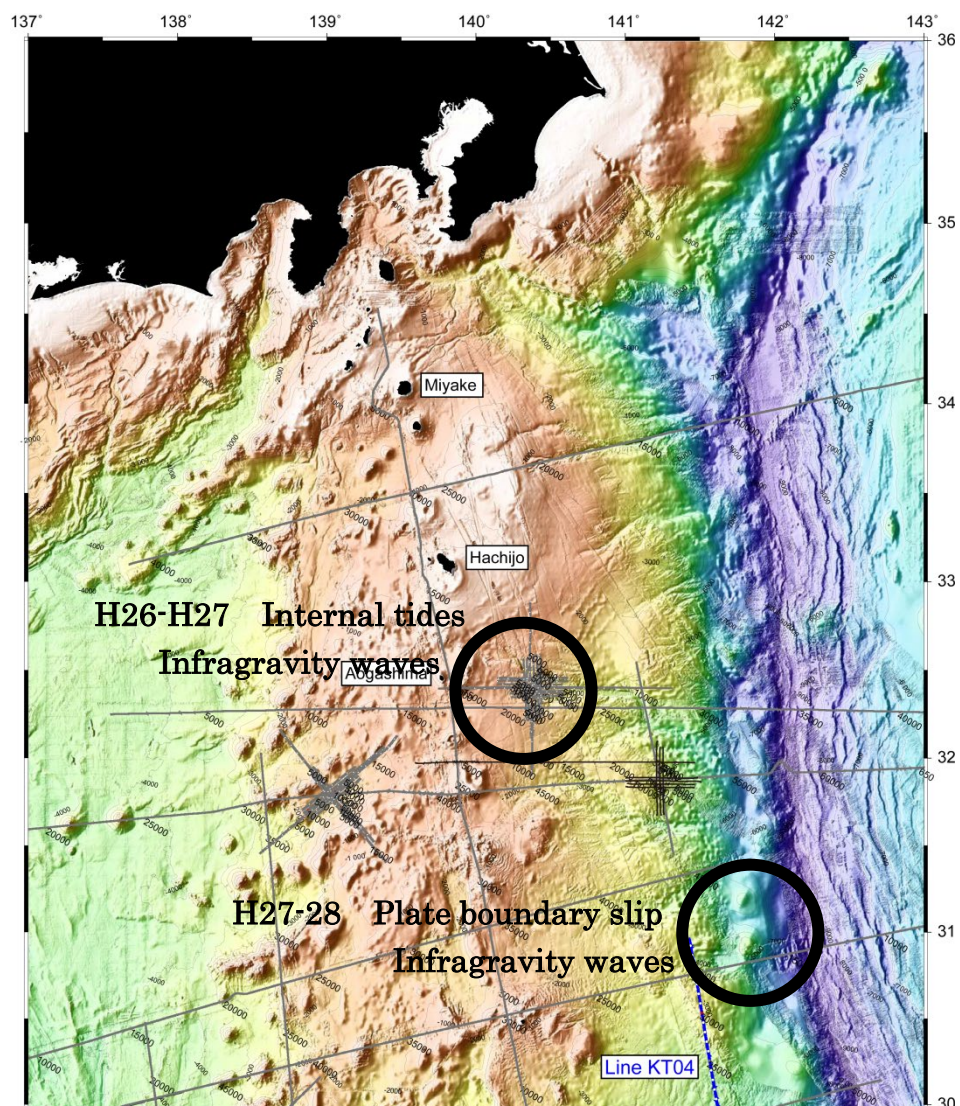


- Future plans

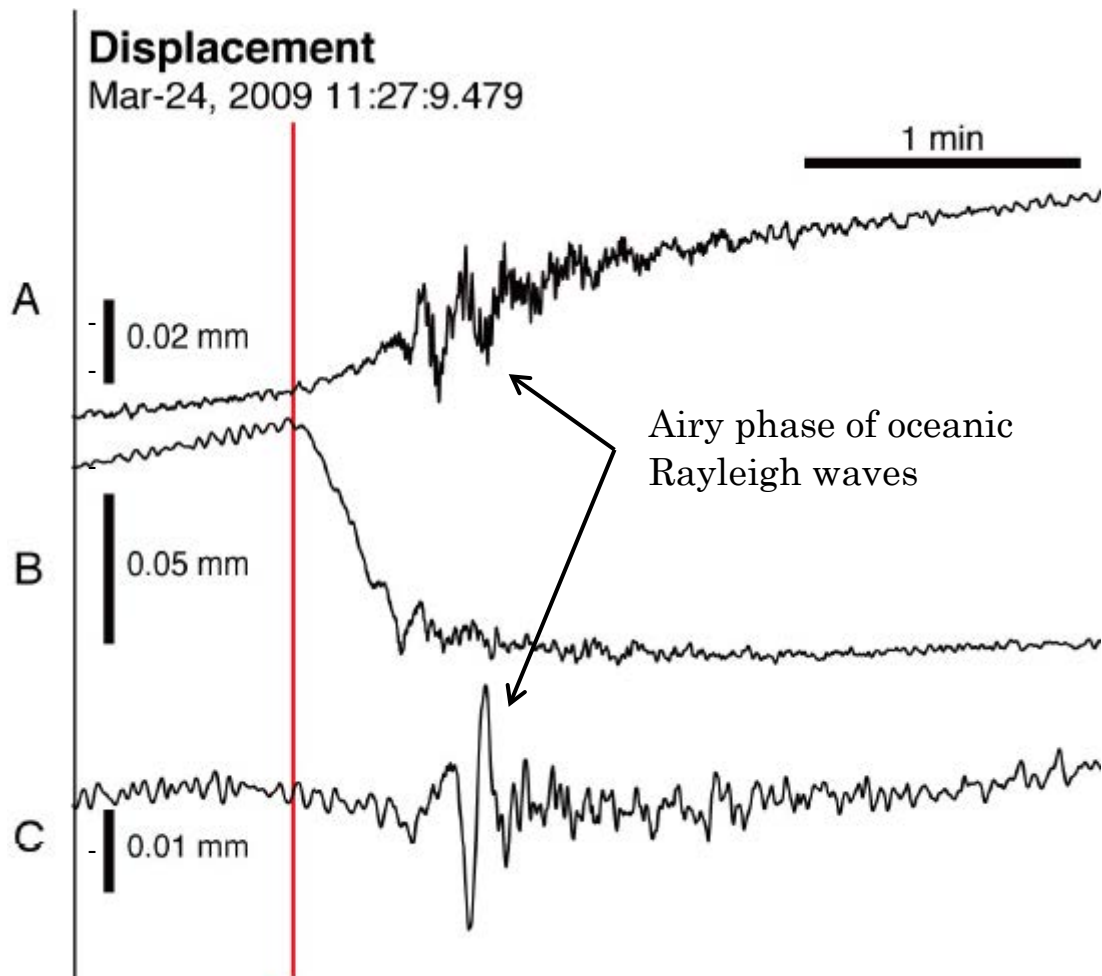
The survey this time is emphasized on one-year observation of processes occurring mainly in the ocean, including internal tides and infragravity waves, using the array of 10 high-resolution pressure gauges placed at the sea bottom off east of Aogashima. The next survey is planned to target on one-year observation of processes occurring mainly inside the Earth using the same observational system. The target area is marked by ellipse in the following map, where the thrust-type seismic activity is unusually high in this particular area of the Izu-Bonin subduction zone.



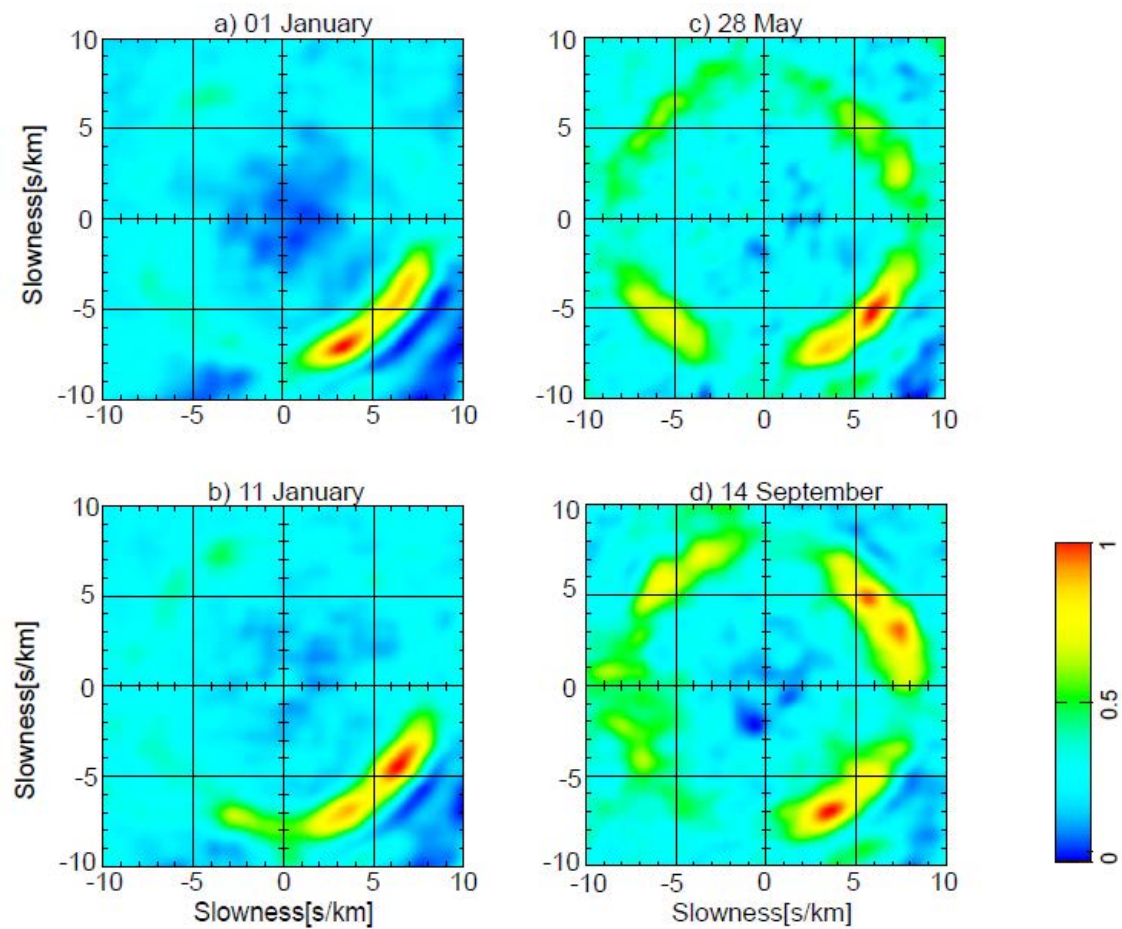
We for this reason plan to apply the form for the use of a JAMSTEC research vessel in the FY2015 to recover the observational system now deployed off east of Aogashima, to retrieve the data, check the instruments and prepare for the next installation on board and to deploy the observation system on the seafloor in the next target area, about 200 km to the southeast of the currently observing area. The new target area is slightly inward of the Bonin trench, as shown in the next map, where the plate subduction is considered to occur mostly in aseismic mode.



The main observational target is the event-like plate boundary slip, which may be detected by observing the oceanic Rayleigh waves in Airy phase with dominant periods of about 10 s, as shown in the next figure. The array of high resolution pressure gauges could detect even slower plate boundary slip that excites seismic waves poorly/



We will also try to locate the excitation sources of infragravity waves using this pressure gage array and that of the DONET of JAMSTEC simultaneously. We have so far determined the direction of the excitation sources of infragravity waves using the pressure gage array of the DONET, as demonstrated below (Tono et al. EPS, 2014 under review). Joint use of the two arrays will make it possible to locate the excitation sources.



#### **4. Notice on Using**

Notice on using: Insert the following notice to users regarding the data and samples obtained.

This cruise report is a preliminary documentation as of the end of the cruise.

This report may not be corrected even if changes on contents (i.e. taxonomic classifications) may be found after its publication. This report may also be changed without notice. Data on this cruise report may be raw or unprocessed. If you are going to use or refer to the data written on this report, please ask the Chief Scientist for latest information.

Users of data or results on this cruise report are requested to submit their results to the Data Management Group of JAMSTEC.

LETTER

Open Access

# Source characteristics of ocean infragravity waves in the Philippine Sea: analysis of 3-year continuous network records of seafloor motion and pressure

Yoko Tono<sup>1\*</sup>, Kiwamu Nishida<sup>2</sup>, Yoshio Fukao<sup>3</sup>, Akiko To<sup>3</sup> and Narumi Takahashi<sup>3</sup>

## Abstract

Continuous 3-year records of broadband ocean-bottom seismometers and pressure gauges of the seafloor network (Dense Oceanfloor Network System for Earthquakes and Tsunamis (DONET)) in the Nankai Trough region made it possible to monitor incoming ocean infragravity (IG) waves. Application of a slant-stacking technique revealed that the most energetic IG waves are incoming across the Nankai Trough from the Philippine Sea with limited energy of reflected waves back from the nearest coast. The sources of the most energetic waves are narrowly and stably localized into two closely adjacent azimuthal windows with mutually different wave spectral characteristics. Both sources show a seasonal variation, weak in summer and strong in winter. Although less energetic, IG waves propagating parallel to the trough and coast are observed. Such waves are greatly amplified when IG waves from a distant typhoon are incoming to the trough, suggesting the secondary origin of IG waves that can emit even more energetic waves than the originally incoming waves.

**Keywords:** Infragravity wave; Seafloor network; Pressure gauge; BBOBS; DONET; Philippine Sea

## Findings

### Introduction

Ocean infragravity (IG) waves are sea surface gravity waves with periods of several minutes and wavelengths of tens of kilometers. The phase velocity of IG waves observed in deep ocean environments is accurately explained by the gravity wave theory (e.g., Webb et al. 1991). These waves are considered to be excited by non-linear interactions between oceanic swells (Longuet-Higgins and Stewart 1962; Herbers et al. 1995) and may be enhanced by tidal modulation in coastal oceans (Guza and Thornton 1982; Okihiro and Guza 1995; Tomson et al. 2006) and deep sea (Sugioka et al. 2010). IG waves also are considered to excite the Earth's hum (Rhie and Romanowicz 2004, 2006; Tanimoto 2005; Nishida et al. 2008; Fukao et al. 2010; Nishida 2013).

Dolenc et al. (2005) compared the power spectra of ocean-bottom seismic records at a station located offshore of the Monterey Bay in California with the wave spectral densities measured by the nearby National Oceanic and Atmospheric Administration (NOAA) buoy. They observed two types of IG wave modulations with short (30- to 40-s) and long (10-day) periods, the latter being correlated with the ocean tides at the station. Sugioka et al. (2010) also observed the tidal modulation of IG waves on the records of broadband ocean-bottom seismometers (BBOBS) at deep seafloors. They further found a remarkable correlation of the IG spectral peak with the seafloor depth. Godin et al. (2013) showed a pronounced dependence of the energy density of IG wave on the frequency and local water depth using pressure gauge records of 28 locations on the seafloor off New Zealand. Harmon et al. (2012) used five differential pressure gauges located off the coast of Sumatra and applied an array analysis. They detected IG waves that propagate along the coast from southeast or south. Crawford et al. (1991) took advantage of a simultaneous measurement of sea-bottom pressure and seafloor displacement at

\* Correspondence: tonojamstec.go.jp

<sup>1</sup>Department of Deep Earth Structure and Dynamics Research, Japan Agency for Marine-Earth Science and Technology, 3173-25, Showa-machi, Kanazawa-ku, Yokohama, Kanagawa 236-0001, Japan

Full list of author information is available at the end of the article

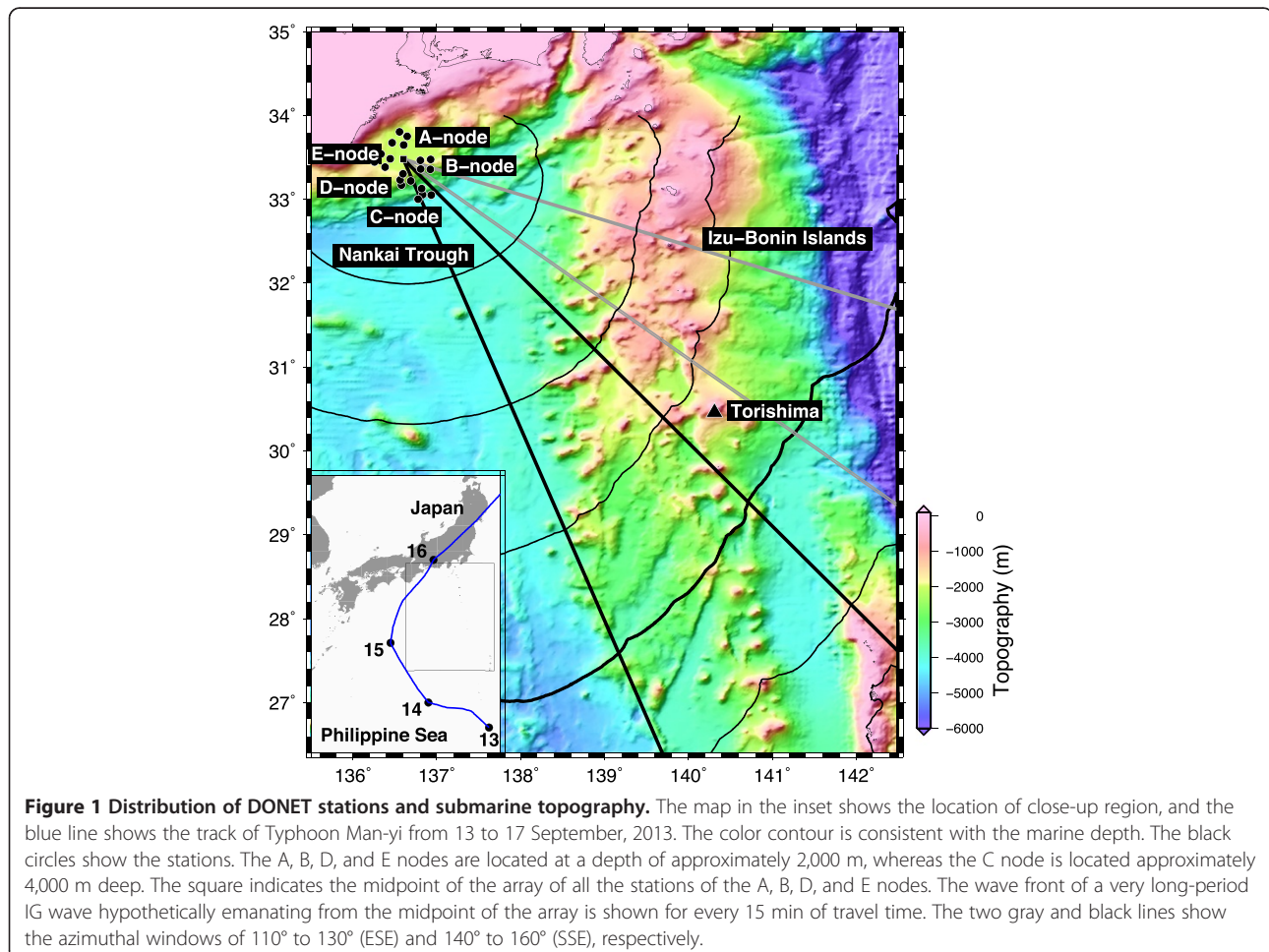
a single station. They measured the sea-bottom pressure changes due to IG waves and the resultant seafloor vertical displacement to take their ratio (compliance) which carries information about the elastic structure of the oceanic crust. When we analyze the sea-bottom pressure and/or seafloor displacement, IG waves, a ubiquitous phenomenon on the sea, can be a strong background noise. Understandings of IG wave-related phenomena are important from the view point of seismology as well as oceanography.

A submarine cable network named the Dense Ocean-floor Network System for Earthquakes and Tsunamis (DONET) was recently deployed offshore of the Kii Peninsula in the Nankai Trough region (Kaneda 2010; Kawaguchi et al. 2010; Nakano et al. 2013). This network is equipped with six instruments at each station, including a three-component BBOBS and an absolute pressure gauge. Thus, DONET provides a good opportunity for array-based compliance analysis to study the crustal structure beneath the network, the generation mechanisms of IG waves, and the IG wave-related seismic phenomena including the Earth's hum. In this study, we

investigate the nature of incoming IG waves to DONET on the basis of continuous 3-year observations.

#### Data and method

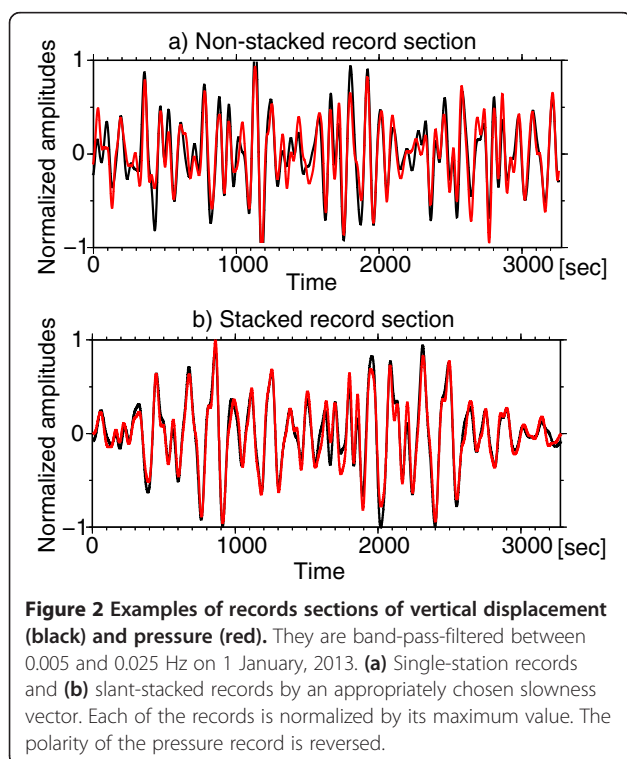
DONET is an ongoing project and currently consists of five nodes, each of which consists of four stations. Figure 1 shows the station distribution of this network and the seafloor topography in the Izu-northern Bonin region. The station interval is 15 to 20 km, on the order of the wavelengths of targeted IG waves of our interest. The four stations at C node are set at seafloor depths between 3,500 and 4,400 m, while 16 stations at other nodes are positioned at depths between 1,900 and 2,500 m. The average of theoretical phase velocities of IG wave calculated at a period of 120 s for all stations is 135 m/s with a standard deviation of 14 m/s, while the average of phase velocities at the same period for 16 stations at other nodes is 129 m/s with a standard deviation of 4 m/s. We regarded the 16 stations as an array and analyzed the records of broadband ocean-bottom seismometers (Guralp CMG-3 T, Guralp Systems, Reading, UK) and quartz pressure gauges (Paroscientific, Inc., Redmond, WA, USA) from January



2011 to December 2013. For each station, both records were band-pass-filtered between 0.005 and 0.025 Hz and were corrected for the instrumental response. Both displacement and pressure time series were divided into segments of 3,600 s with an overlap of 1,800 s. Segments including earthquake signals, artificial noise, and boisterous noise disturbances due to extreme weather or nearby typhoon activity were discarded. The record sections at various stations were mutually shifted according to a presumed slowness vector and were then stacked. Each slant-stacked record section was auto-correlated and Fourier-transformed to obtain a power spectrum. The same procedure was repeated with numerous slowness vectors to obtain a two-dimensional frequency-slowness spectrum (e.g., Rost and Thomas 2002; Nishida et al. 2005), and all similarly obtained spectra for 1 day were stacked. The pressure records were similarly processed. The power spectral density (PSD) of either seafloor displacement or pressure was averaged over the analyzed frequency range to obtain the average PSD as a slowness vector function. We searched for the slowness vector that maximizes the average PSD. The direction and amplitude of such a slowness vector were regarded as the incident azimuth and apparent slowness of the incoming IG waves, respectively.

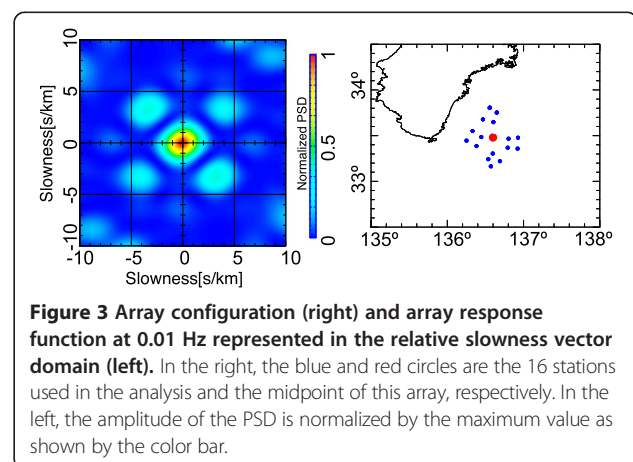
## Result

Figure 2a shows an example of the comparison of the seafloor records of vertical displacement (black) and pressure (red). Both were band-pass-filtered between



0.005 and 0.025 Hz and were normalized by the maximum amplitude of each trace, and the polarity of the pressure record was reversed. The agreement between the two traces was remarkable, which was expected if the signal is an IG wave whose phase velocity is much lower than that of a seismic wave (Crawford et al. 1991). Figure 2b shows an example of comparison of the stacked records of vertical displacement (black) and pressure (red). Stacking was accomplished by using a slowness vector that makes the stacked IG wave most energetic. The determined slowness value was consistent with that expected from the seafloor depth and the observed frequency range. This consistency, coupled with the remarkable waveform match shown in Figure 2, offered the most direct support for our interpretation of the observed disturbance as the IG waves. The station configuration and the response function of this array at 0.01 Hz (Rost and Thomas, 2002) are shown in Figure 3. The response function is represented in the slowness vector domain, where its spread around the origin indicates how narrowly in absolute value and how unbiasedly in azimuthal direction the slowness vector can be constrained by the array. The response function of our array is sharp and isotropic enough to warrant further analyses.

Figure 4 shows four examples of the average PSD distribution in the slowness vector domain. Highly similar diagrams were also obtained for seafloor displacement fluctuation, as expected from the waveform match between the displacement and pressure records (Figure 2). Figure 4a,b shows typical patterns in winter, Figure 4c shows the typical pattern in spring, and Figure 4d shows a pattern when a typhoon was located in the Philippine Sea approximately 1,000 km to the south of the network. All the figures show a relatively large power between two dashed circles with slowness values of 7 and 9 s/km, or phase velocity values of 140 and 110 m/s, respectively, indicating that the observed waves are IG waves within a



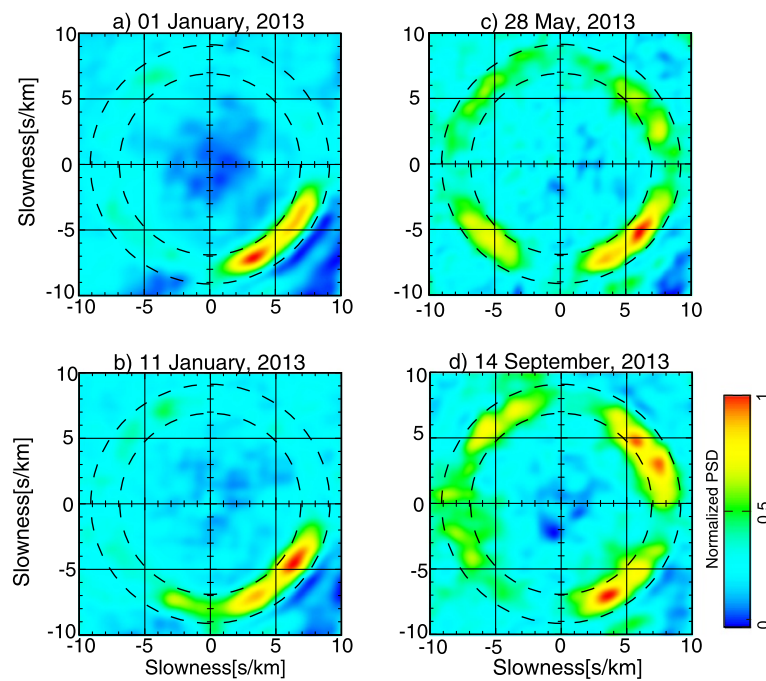


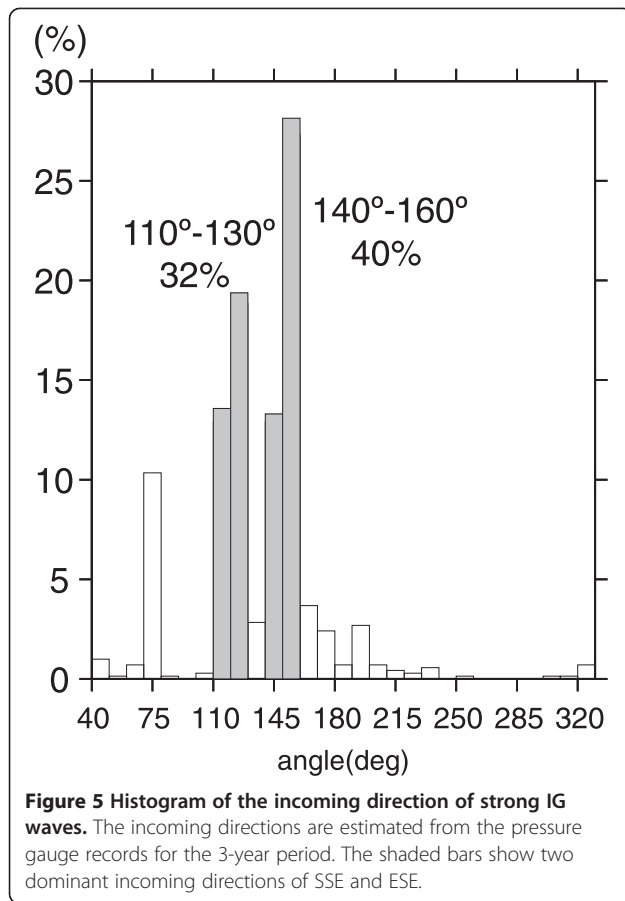
**Figure 4** Four examples of the average PSD distribution in the slowness vector domain. The average of PSD is taken over a frequency range between 0.005 and 0.025 Hz. The recorded day is shown at the top of each diagram. The radii of two dashed circles indicate the slowness values of 7 and 9 s/km. The amplitudes of the PSDs in each diagram are normalized by their maximum value. The slowness (incoming direction, velocity) values estimated from the position of the red peak are **(a)** 7.9 s/km (153°, 127 m/s); **(b)** 7.8 s/km (125°, 128 m/s), **(c)** 8.0 s/km (131°, 126 m/s), and **(d)** 7.8 s/km (153°, 128 m/s).

frequency range of 0.005 to 0.025 Hz propagating through the ocean at depths around 2,000 m. The IG signal intensity is persistently highest for the incoming waves crossing the Nankai Trough from the southeast (SE). This incoming direction actually consists of two closely adjacent directions: the south-southeast (SSE) and east-southeast (ESE) (see Figure 5 for a histogram of the measured incoming direction). Waves from the SSE direction through the deeper ocean are usually more energetic (Figure 4a) but are at times less energetic (Figure 4b) than those from the ESE direction through the shallower ocean (see Figure 1). These waves, either from SSE or ESE, are particularly strong in winter (see Figure 6).

An example of the typical pattern in spring (and summer) is shown in Figure 4c, where the waves from the SE reduce their intensity so that wave signals from the other directions, particularly from the southwest (SW) and from the northeast (NE) to east-northeast (ENE), become more visible. These waves may be interpreted as edge waves trapped by reflections from the coast and refractions backward from the Nankai Trough to propagate through the corridor in between. Figure 4d shows the impact of Typhoon Man-yi on 14 September, 2013, where it was located on the Philippine Sea far to the south of the network as sketched in the inset of Figure 1 (Japan Meteorological Agency (JMA); [www.jma.go.jp/](http://www.jma.go.jp/)

[jma/jma-eng/jma-center/rsmc-hp-pub-eg/trackarchives.html](http://jma/jma-eng/jma-center/rsmc-hp-pub-eg/trackarchives.html)). This typhoon moved from a back azimuth of 175° to 193° during the day and amplified the IG waves incoming from the SSE direction, and even more greatly from the NE to ENE direction, whereas those incoming from the ESE remained weak. Strengthening of IG waves from the NE to ENE direction is commonly observed when a typhoon is reported to be on the Philippine Sea, regardless of the exact incoming direction of IG waves originated by the typhoon, which varies widely in a range between the SSE and SW. These observations suggest that the amplified IG waves from the NE to ENE direction were generated secondarily at far distances from the primary (typhoon) source.

We measured the incoming direction of the most energetic IG waves during the 3-year period. In the subsequent discussion, we show only the results from the pressure records, which are in agreement with those from the displacement records within an error of 5°. Figure 5 shows a histogram of the measured incoming direction. The SE direction dominates, although the detail is composed of two closely adjacent directions with a clear gap in between: one is SSE in a range of 140° to 160° (measured clockwise from the north) and the other is ESE in a range of 110° to 130°, which account for 40% and 32% of the total measurements, respectively. Together, these two



directions account for 72% of the measurements. Figure 6a shows the daily variations of the incoming direction of the most energetic IG waves throughout the 3 years, where the color indicates the PSD value. The seasonal variations of the incoming directions are clarified by Figure 6b, in which the results for each of 3 years are superimposed. Several features can be observed from this figure: (1) The SSE and ESE persist as the dominant incident directions; (2) the energy of the IG wave incoming from these two directions shows the same seasonal variations of strong in winter and weak in summer; and (3) in summer, strong waves occasionally are incoming from the other directions. To explore observation (3) in detail, we divided the plots in Figure 6b into two as Figure 6c,d. The plots in Figure 6d are limited to the days on which the JMA reported a typhoon or typhoons on the Philippine Sea, whereas the plots in Figure 6c exclude such days. Figure 6c reinforces observations (1) and (2), which imply two distinct excitation sources of IG waves which are spatially stable and seasonally varying synchronously. Figure 6d indicates that the typhoon-associated IG waves are incoming from separate directions, one more or less directly from the typhoon in the SSE (as shown in Figure 4d) to SW and the other apparently from the

submarine topographic high in the NE to ENE. IG waves incoming from this direction are often more energetic than those directly from the source on the typhoon's track. It is noted that the wave amplitudes from the two stationary sources in the SSE and ESE directions remained largely unchanged, even in the days where a typhoon was reported to be on the Philippine Sea.

### Discussion

We have identified two distinct excitation sources of IG waves in the SSE and ESE directions away from the network. Figure 7 shows that the IG waves from these two sources have different spectral characteristics. If we search for the source using the lower-frequency components (0.005 to 0.01 Hz), it is dominantly located in the SSE window (140° to 160°) as shown in Figure 7a, which accounts for 60% of the total measurements. If, on the other hand, search is made for the source using the higher-frequency components (0.01 to 0.025 Hz), it is dominantly located in the ESE window (110° to 130°) as shown in Figure 7b, which accounts for 52% of the total measurements. Clearly, lower-frequency IG waves are incoming more dominantly from the SSE than from the ESE. Higher-frequency IG waves are incoming more dominantly from the ESE than SSE but also include other incoming directions of 40° to 80° (16%), 190° to 230° (13%), and 300° to 330° (2%). The signal intensities in the higher frequency range are in general weaker than those in the lower frequency range as shown by the difference of detected IG wave PSD amplitude. This is in part because the higher-frequency IG wave decreases its amplitude more rapidly with depth than the lower-frequency IG wave. Although Figure 4c,d shows relatively large power in the NW direction (300° to 330°), the waves from this direction are usually very weak as compared to those from the SE direction (Figure 4a,b). The most energetic waves incoming from the SE direction are poorly accompanied by reflections from the nearest coast, where wave scattering, wave-wave conversion, and dissipation may be significant. As illustrated in Figure 1, the ocean in the ESE window is shallower with larger and more densely populated islands, whereas the ocean in the SSE window is deeper with smaller and more sparsely populated islands. We suggest that the spectral difference between the two azimuthal windows (Figure 7) reflects these differences in seafloor topography, which should affect the processes of generation and propagation of IG waves. In Figure 1, we added the inverse refraction diagram for a very long IG wave incoming to the array, which was obtained by combining the Tsunami Travel Times (TTT) software (Wessel 2009) with the bathymetry data of ETOPO1 ([www.ngdc.noaa.gov/mgg/global/global.html](http://www.ngdc.noaa.gov/mgg/global/global.html)). This diagram demonstrates that the wave front of the long IG wave in the

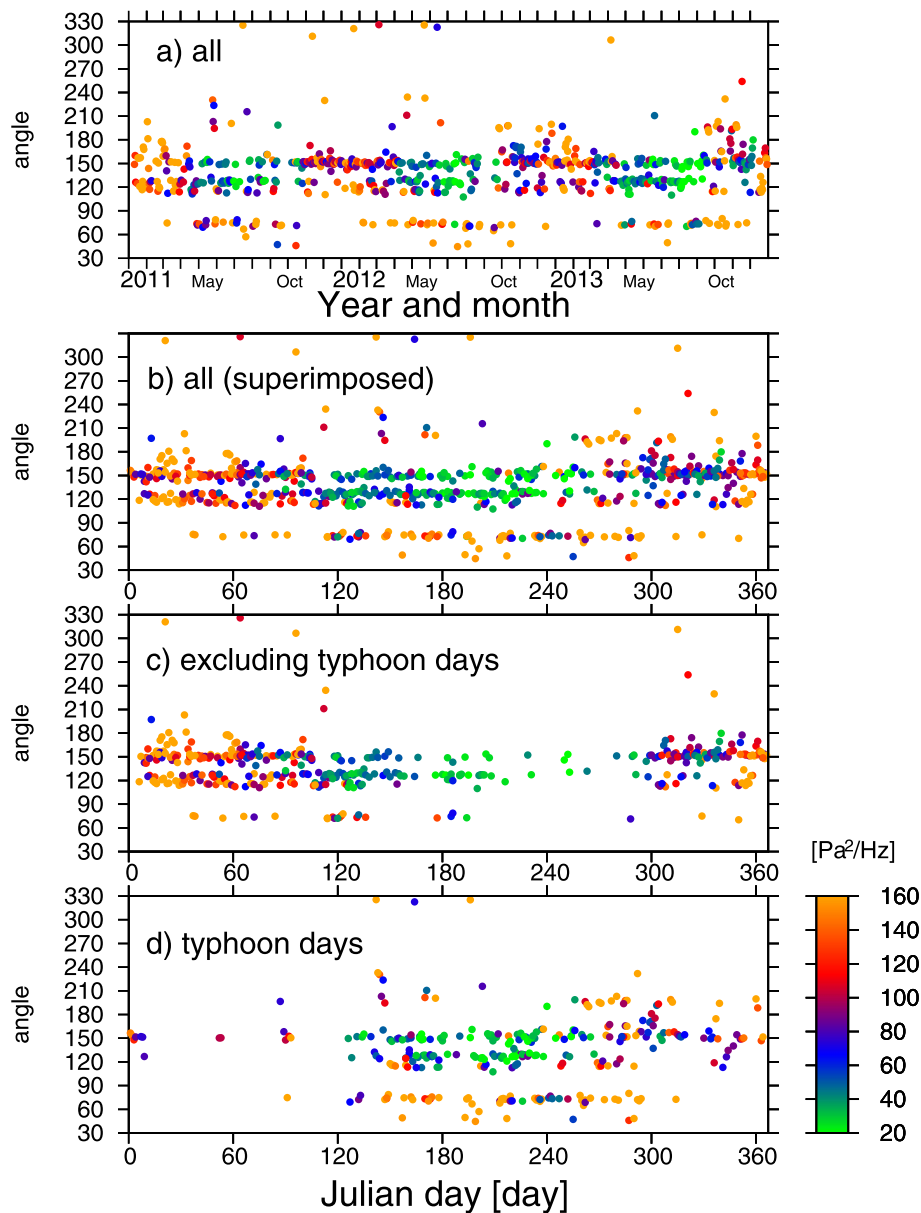
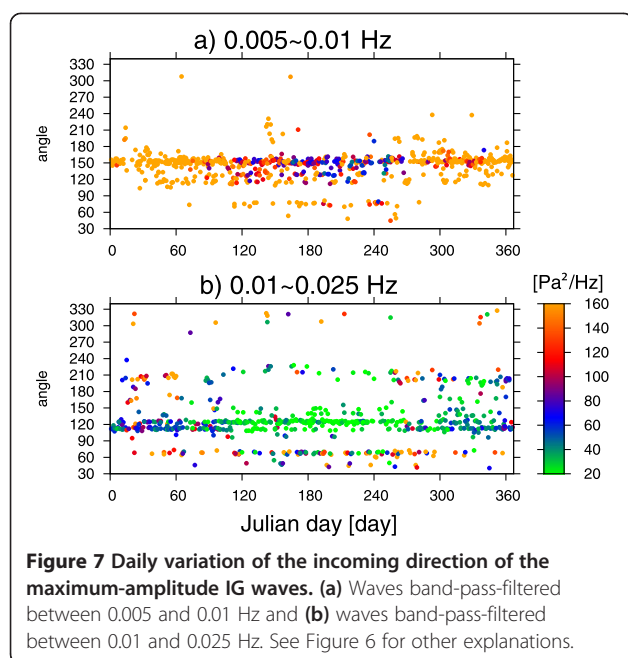


**Figure 6** Daily variation of the incoming direction of the maximum-amplitude IG waves. The color indicates the maximum amplitude measured in terms of the average PSD between 0.005 and 0.025 Hz. **(a)** Results through the entire 3-year period. **(b)** Results for each year plotted on the same Julian day. **(c)** Results excluding days in which the Japan Meteorological Agency reported a typhoon or typhoons in the Pacific. **(d)** Results for days in which a typhoon or typhoons existed in the Pacific.

ESE widow is more strongly distorted by the seafloor complexity than that in the SSE window. Although the DONET alone cannot locate the sources in the ESE and SSE windows, installation of a temporal seafloor array in the southeast window, e.g., near the Torishima Island (Figure 1), may suffice to determine these two source locations simultaneously.

Besides the stationary sources discussed above, IG waves can be generated sporadically by extreme weather, typically by typhoons. The incoming direction of the

typhoon-originated IG waves depends in a seemingly complex way on the past track of the moving typhoon, as shown in the inset of Figure 1. Most unexpectedly, a typhoon to the south far from the network always enhances IG waves incoming from the NE to ENE direction (Figure 6d). The enhanced IG waves are often more energetic than those directly from the source region (Figure 4d), suggesting some amplification mechanism at the secondary source at distances far away from the primary source.



## Conclusion

Although IG waves are known to be a ubiquitously observable phenomenon (Webb et al. 1991), this does not necessarily mean that IG waves are generated everywhere in the ocean. We have identified persistent, energetic IG sources in two azimuthal windows SSE and ESE of the network. The identified sources are rather localized and remain geographically stationary but show seasonally varying intensities of strong in winter and weak in summer. Higher-frequency waves are more dominantly incoming from the shallower ocean with more complex seafloor topography in the ESE direction. Lower-frequency waves are more dominantly incoming from the deeper ocean with less complex seafloor topography in the SSE direction. As shown in Figures 4c and 7b, an additional remarkable observation was the persistence of feeble IG waves incoming from the SW direction and from the NE-ESE directions, which may be interpreted as edge waves generated by reflections from the coast and refractions backward from the Nankai Trough to propagate as trapped waves in between. In particular, IG waves incoming from the NE-ESE directions are greatly amplified when IG waves originated by a typhoon on the Philippine Sea are incident. The amplified amplitudes often well exceed the amplitudes of incident waves from the primary origin. A seafloor network equipped with broadband ocean-bottom seismometers and pressure gauges, such as the DONET, is highly useful for detecting IG waves and observing the related phenomena.

## Competing interests

The authors declare that they have no competing interests.

## Authors' contributions

YT, KN, and YF conceived and designed the study; AT and NT acquired the data; YT, KN, and YF performed the analysis and interpretation of data; YT drafted the manuscript; and YF made a critical revision of the manuscript. All authors read and approved the final manuscript.

## Acknowledgements

The Generic Mapping Tools (Wessel and Smith 1991) and Seismic Analysis Code (Goldstein et al. 1998) were used in this study. A part of the DONET data is available from <http://www.jamstec.go.jp/donetevent/NINJA/top.do>. We thank Dai Suetsugu for all his help. We also thank two anonymous reviewers and the associate editor (Azusa Nishizawa) for many constructive comments.

## Author details

<sup>1</sup>Department of Deep Earth Structure and Dynamics Research, Japan Agency for Marine-Earth Science and Technology, 3173-25, Showa-machi, Kanazawa-ku, Yokohama, Kanagawa 236-0001, Japan. <sup>2</sup>Earthquake Research Institute, University of Tokyo, 1-1-1, Yayoi, Bunkyo-ku, Tokyo 113-0032, Japan. <sup>3</sup>Research and Development Center for Earthquake and Tsunami, Japan Agency for Marine-Earth Science and Technology, 3173-25, Showa-machi, Kanazawa-ku, Yokohama, Kanagawa 236-0001, Japan.

Received: 6 June 2014 Accepted: 16 August 2014

Published: 26 August 2014

## References

- Crawford WC, Webb SC, Hildebrand JA (1991) Seafloor compliance observed by long-period pressure and displacement measurements. *J Geophys Res* 96:16,151–16,160, doi:10.1029/91JB01577
- Dolenc D, Romanowicz B, Stakes D, McGill P, Neuhauser D (2005) Observations of infragravity waves at the Monterey ocean bottom broadband station (MOBB). *Geochem Geophys Geosyst* 6, Q09002, doi:10.1029/2005GC000988
- Fukao Y, Nishida K, Kobayashi N (2010) Seafloor topography, ocean infragravity waves, and background Love and Rayleigh waves. *J Geophys Res* 115, B04302, doi:10.1029/2009JB006678
- Godin OA, Zabotin NA, Sheehan AF, Yang Z, Collins JA (2013) Power spectra of infragravity waves in a deep ocean. *Geophys Res Lett* 40:2159–2165, doi:10.1002/grl.50418
- Goldstein P, Dodge D, Firpo M, Ruppert S (1998) What's new in SAC2000? Enhanced processing and database access. *Seismological Research Lett* 69:202–205
- Guza RT, Thornton EB (1982) Swash oscillations on a natural beach. *J Geophys Res* 87:483–491, doi:10.1029/JC087C01p00483
- Harmon N, Henstock T, Srokosz M, Tilmann F, Rietbrock A, Barton P (2012) Infragravity wave source regions determined from ambient noise correlation. *Geophys Res Lett* 39, L04604, doi:10.1029/2011GL050414
- Herbers THC, Elager S, Guza RT (1995) Generation and propagation of infragravity waves. *J Geophys Res* 100:24,863–24,872, doi:10.1029/95JC02680
- Kaneda Y (2010) The advanced ocean floor real time monitoring system for mega thrust earthquakes and tsunamis. In: Application of DONET and DONET2 data to seismological research and disaster mitigation, MTS/IEEE OCEANS 2010
- Kawaguchi K, Araki E, Kaneko S, Nishida T, Komine T (2010) Subsea engineering ROV and seafloor observatory construction. In: Proceedings of international symposium on underwater technology 2010/international workshop on scientific use of submarine cables and related technologies 2010, SSC11-1019, CD-ROM
- Longuet-Higgins MS, Stewart RW (1962) Radiation stress and mass transport in gravity waves, with application to 'surf beat'. *J Fluid Mech* 13:481–504
- Nakano M, Nakamura T, Kamiya S, Ohori M, Kaneda Y (2013) Intensive seismic activity around the Nankai trough revealed by DONET ocean-floor seismic observations. *Earth Planets Space* 65:5–15, doi:10.5047/eps.2012.05.013
- Nishida K (2013) Earth's background free oscillations. *Annu Rev Earth Planet Sci* 41:719–740, doi:10.1146/annurev-earth-050212-124020
- Nishida K, Kawakatsu H, Fukao Y, Obara K (2008) Background Love and Rayleigh waves simultaneously generated at the Pacific Ocean floors. Source distribution of Earth's background oscillations. *Geophys Res Lett* 35:L16307
- Nishida K, Fukao Y, Watada S, Kobayashi N, Tahira M, Suda N, Nawa K, Oi T, Kitajima T (2005) Array observation of background atmospheric waves in the

- seismic band from 1 mHz to 0.5 Hz. *Geophys J Int* 162:824–840, doi:10.1111/j.1365-246X.2005.02677.x
- Okiihiro M, Guza RT (1995) Infragravity energy modulation by tides. *J Geophys Res* 100:16,143–16,148, doi:10.1029/95JC01545
- Rhie J, Romanowicz B (2006) A study of the relation between ocean storms and the Earth's hum. *Geochem Geophys Geosyst* 7, Q10004, doi:10.1029/2006GC001274
- Rhie J, Romanowicz B (2004) Excitation of Earth's continuous oscillations by atmosphere–ocean–seafloor coupling. *Nature* 431:552–556, doi:10.1038/nature02942
- Rost S, Thomas C (2002) Array seismology: methods and applications. *Rev Geophys* 40(3):1008, doi:10.1029/2000RG000100
- Sugioka H, Fukao Y, Kanazawa T (2010) Evidence for infragravity wave-tide resonance in deep oceans. *Nat Commun* 1:84, doi:10.1038/ncomms1083
- Tanimoto T (2005) The oceanic excitation hypothesis for continuous oscillations of the Earth. *Geophys J Int* 160:276–288, doi:10.1111/j.1365-246X.2004.02484.x
- Tomson J, Elgar S, Raubenheimer B, Herber THC, Guza RT (2006) Tidal modulation of infragravity waves via nonlinear energy losses in the surfzone. *Geophys Res Lett* 33, L05601, doi:10.1029/2005GL025514
- Webb SC, Zhang X, Crawford W (1991) Infragravity wave in the deep ocean. *J Geophys Res* 96:16,151–16,160, doi:10.1029/90JC02212
- Wessel P (2009) Analysis of observed and predicted tsunami travel times for the Pacific and Indian oceans. *Pure Appl Geophys* 166(1–2):301–324
- Wessel P, Smith WHF (1991) Free software helps map and display data. *Eos Trans AGU* 72:441

doi:10.1186/1880-5981-66-99

**Cite this article as:** Tono et al.: Source characteristics of ocean infragravity waves in the Philippine Sea: analysis of 3-year continuous network records of seafloor motion and pressure. *Earth, Planets and Space* 2014 **66**:99.

**Submit your manuscript to a SpringerOpen<sup>®</sup> journal and benefit from:**

- Convenient online submission
- Rigorous peer review
- Immediate publication on acceptance
- Open access: articles freely available online
- High visibility within the field
- Retaining the copyright to your article

---

Submit your next manuscript at ► [springeropen.com](http://springeropen.com)

---